Compontent Tolerance Effect on Ultra-Wideband Low-Noise Amplifier Performance

Adriana Serban, Magnus Karlsson and Shaofang Gong

Adriana Serban, Magnus Karlsson and Shaofang Gong, Compontent Tolerance Effect on Ultra-Wideband Low-Noise Amplifier Performance, 2011, IEEE Transactions on Advanced Packaging, (33), 3, 660-668.
http://dx.doi.org/10.1109/TADVP.2010.2041348

Component Tolerance Effect on Ultra-Wideband Low-Noise Amplifier Performance

Adriana Serban, Magnus Karlsson, and Shaofang Gong, *Member, IEEE*

***Abstract*—A study of the component tolerances on an ultra-wideband (UWB) low-noise amplifier designed on a conventional printed circuit board is presented in this paper. The low-noise amplifier design employs dual-section input and output microstrip matching networks for wideband operation with a low noise figure and a flat power gain. First, the effect of passive component and manufacturing process tolerances on the low-noise amplifier performance is theoretically studied by means of sensitivity analyses. Second, simulation and measurement results are presented for verification of the analytical results. It is shown that, compared with a lumped matching network design, a microstrip matching network design significantly reduces the UWB low-noise amplifier sensitivity to component tolerances.**

***Index Terms*—Low-noise amplifier (LNA), matching networks, sensitivity analysis, ultra-wideband (UWB).**

I. Introduction

THE low-noise amplifier (LNA) for ultra-wideband (UWB) radio systems is one of the most critical components in the radio front-end. Due to the characteristics of UWB signals, i.e., very low radiated power (-41.3 dBm/MHz) and large bandwidth, a UWB receiver requires better receiver sensitivity and a lower noise figure than, for example, an IEEE 802.11a receiver [1]. The expected receiver sensitivity can be achieved by an optimal design of the LNA in terms of a near-to-minimum noise figure and reasonable power gain over the entire band. On one hand, classical wideband amplifier topologies, e.g., feedback [2], [3] and distributed amplifiers [4], [5], have difficulty to meet all the requirements of a near-to-minimum noise figure, low-power consumption, small area, and low cost. On the other hand, an LNA implemented with multisection matching networks provides more degrees-of-freedom to achieve both a low noise figure and flat power gain without increasing the power consumption [6], [7]. However, as the multisection input and output matching networks have more circuit components, the LNA noise figure and power gain can be more sensitive to the statistical variations of the passive components, either they are lumped inductors and capacitors or distributed passives, e.g., using microstrip transmission lines.

Manuscript received April 15, 2009; revised July 05, 2009; accepted December 13, 2009. This work was supported by SonyEricsson and Vinnova. This work was recommended for publication by Associate Editor R.-B. Wu upon evaluation of the reviewers comments.

The authors are with the Linköping University, SE-60174 Norrkoping, Sweden (e-mail: adrse@itn.liu.se).

Color versions of one or more of the figures in this paper are available online at http://ieeexplore.ieee.org.

Digital Object Identifier 10.1109/TADVP.2010.2041348

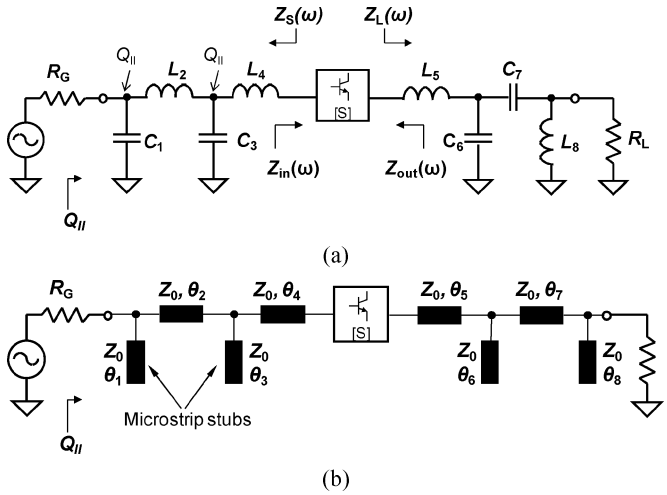

Fig. 1. Multisection UWB LNA topologies with (a) lumped and (b) distributed matching networks. Q_{II} is the loaded Q-factor.

From our previous radio-frequency (RF) circuit designs, i.e., antenna [8], [9], frequency-triplexer [10], narrowband and UWB LNAs [11], [12], antenna-LNA co-design [13], [14] and UWB bias networks [15] as well as considering the passive component tolerance problem, two interesting observations were found. First, using distributed components of microstrips, very good agreement was obtained between simulated and measured results. Second, the measured circuit parameters have shown low variation from circuit to circuit under test. However, this approach to use distributed components on a printed circuit board has rarely been used in RF front-end circuit design for wideband applications, mainly due to a common view that the printed circuit board process requires large manufacturing tolerance and therefore large variation of circuit performance.

In this paper multisection UWB LNA designs with lumped- and distributed-matching networks are studied. The simplified schematics of the two UWB LNA implementations are shown in Fig. 1. First, sensitivity analyses of the noise figure matching condition in response to frequency are done with regard to passive component tolerances. Then, simulations including real-world lumped passive component tolerances, and for the distributed matching networks, manufacturing process tolerances are performed in advanced design system (ADS) from Agilent Technologies, Inc. In order to get a clear picture of how manufacturing tolerances affect RF circuit performance, the LNA with multisection distributed matching networks is designed and manufactured in a commercial printed circuit board process aiming for a low noise figure and a flat power gain over the entire 3.1–4.8 GHz bandwidth.

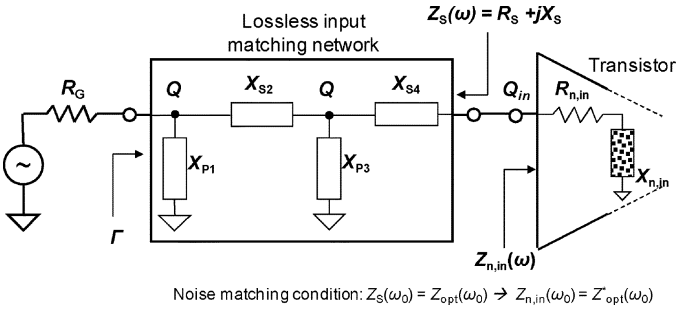

Fig. 2. Circuit model for noise matching condition analysis with dual-section input matching network and transistor equivalent noise impedance.

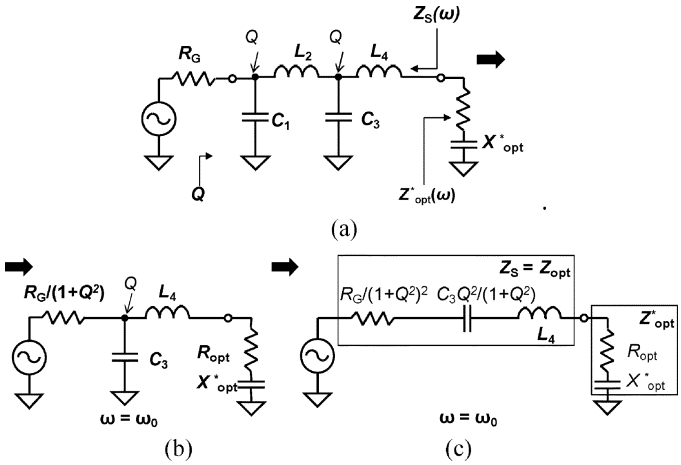

Fig. 3. Series-parallel conversion of a dual-section input matching network at $\omega = \omega_0$.

The simulation results of the UWB LNA with distributed matching networks are verified by experimental results. Finally, the amplifier performance with distributed matching networks on a commercial printed circuit board is discussed and concluded.

II. Sensitivity Analysis of Wideband LNA With Multisection Matching Networks

Passive components, e.g., capacitors, inductors, transformers, and transmission lines, play a key role in determining the overall characteristics of RF circuits [16], [17]. Due to their nominal value tolerances, parasitics and manufacturing process variations, the response of the multisection UWB LNA shown in Fig. 1(a) and (b) is likely to deviate from the results predicted by simulations where only nominal component values and typical mean process parameters are used. It is therefore of interest to know and compare the sensitivity of a multisection UWB LNA implemented with (a) lumped and (b) distributed matching networks.

There are different ways to approach the passive component tolerance problem: 1) statistical analysis using electronic design automation software tools to perform Monte Carlo analysis [18], and 2) sensitivity analysis based on sensitivity functions derived from a given circuit configuration [19]. In this work, the problem of UWB LNA parameter variation due to passive component tolerance is firstly addressed using sensitivity analysis of the matching condition. The cumulative effect of the passive component tolerances on impedance $Z_S(\omega)$ [see Fig. 1(a)] deviation from the designed value is modeled, simulated, and verified by measurement. Other aspects as the problem of via-hole parasitics which can affect the amplifier properties at high frequencies are not treated in this study.

A. Noise-Matching Circuit Model

The effect of the input matching network and its component tolerances on the wideband LNA noise figure can be analyzed considering the circuit model shown in Figs. 2 and 3. In Fig. 2, the input matching network is a lossless dual-section network represented by its parallel and series reactances, X_{P1}, X_{P3}, and X_{S2}, X_{S4}, respectively. It transforms the generator resistor R_G (usually 50 Ω) into a complex source impedance $Z_S(\omega)$, $Z_S(\omega) = R_S(\omega) + jX_S(\omega)$, where R_S and X_S are the resistive and reactive parts of Z_S, as illustrated in Fig. 3(c). The selection of the parallel and series reactances, X_{P1}, $X_{\rm P3}$, and X_{S2}, X_{S4} of the lossless dual-section input matching network in Fig. 2 is not unique. The only restriction is that X_{P1} and X_{S2} and X_{P3} and X_{S4} are of opposite sign. Moreover, depending on the requirements of the application, the input and output matching networks can be implemented as band-pass, low-pass and high-pass filters [12]. For the aim of this study, low-pass matching networks of constant nodal quality factor Q are considered.

The active device, i.e., the transistor, is represented in Fig. 2 by its equivalent input noise impedance $Z_{n,in}(\omega) = R_{n,in}(\omega) + {\rm j}X_{n,in}(\omega)$. In RF and microwave LNA design approaches, the noise matching condition is given as

$$Z_S(\omega) = Z_{\rm opt}(\omega) \tag{1}$$

where $Z_{\rm opt}(\omega)$ is the optimum noise impedance seen towards the generator. $Z_{\rm opt}(\omega)$ is usually a known transistor parameter given by the manufacturer. Hence, using (1), the equivalent noise impedance looking into the transistor can be expressed as $Z_{n,in}(\omega) = Z^*_{\rm opt}(\omega)$, i.e., $R_S = R_{n,in}$ and $X_S = -X_{n,in}$.

However, the noise matching condition (1) occurs only at one frequency ω_0, and (1) becomes $Z_S(\omega_0) = Z_{\rm opt}(\omega_0)$. In a narrow band around the resonance frequency ω_0 the impedance matching condition can be represented by the RLC series equivalent network shown in Fig. 3(c). Moreover, using two parallel-series transformations at $\omega = \omega_0$ [20], [21], the dual-section matching network in Fig. 3(a) can be represented firstly as an equivalent single-section matching network [Fig. 3(b)], and secondly as an equivalent series network [Fig. 3(c)]. In Fig. 3, Q is the loaded Q-factor of the matching network and related to its bandwidth (BW) by $BW_{-3\ {\rm dB}} = \omega_0/Q$, [17]. Following [21], the shunt and series branches [C_1 and L_2 in Fig. 3(a)] are resonant at ω_0. Hence, in Fig. 3(b) only the resistive component $R_G(1 + Q^2)$ driving the rest of the circuit is shown. Finally, the source resistance R_S and source reactance X_S can be expressed as a function of the generator resistance R_G and loaded Q-factor, as shown in Fig. 3(c).

The equivalent network in Fig. 3(c) is further used in Sections II-B and II-C for the analysis of the noise matching condition at $\omega = \omega_0$.

B. Noise-Matching Sensitivity to Component Tolerance

The noise figure degradation due to mismatch from $Z_{\rm opt}$ is usually represented by

$$F(\omega) = F_{\min} + \frac{G_n}{R_S}\{[R_S - R_{\rm opt}(\omega)]^2 + [X_S - X_{\rm opt}(\omega)]^2\} \tag{2}$$

where $F(\omega)$ is the "spot" noise figure, i.e., calculated for a 1-Hz bandwidth at a given frequency and $F_{\min}$ is the amplifier minimum attainable noise figure. G_n is the equivalent noise conductance of the active device ($G_n = 1/R_n$, where R_n is the equivalent noise resistance of the device) [16]. In this study, parameters in (2) are not normalized, hence capitalized.

From (2) it is seen that the noise figure of an amplifier depends on (a) the accuracy of the noise impedance matching, represented by the $\Delta R_S = R_S - R_{\rm opt}$ and $\Delta X_S = X_S - X_{\rm opt}$ and (b) intrinsic noise transistor parameter, G_n. For the aim of this work, G_n, $R_{\rm opt}$ and $X_{\rm opt}$ variation due to the on-wafer process parameter variation is not considered, while R_S and X_S are considered to diverge from their designed (optimal) value due to component and manufacturing process tolerances. Thus, with reference to Fig. 1(a) and Fig. 3, the source impedance Z_S is the result of generator resistance (R_G) transformation and it is a function of all the reactive lumped network components, i.e., $Z_S = f(L_i, C_i), i = 1, 2, 3, 4$. For the distributed matching network case in Fig. 1(b), the source impedance Z_S is a function of the characteristic impedance Z_0 and of the electrical length θ_i of every transmission line in the network, i.e., $Z_S = f(Z_0, \theta_i)$. $\theta_i = \beta l_i$, where β is the propagation constant [16] and l_i is the length of every distributed element in Fig. 1(b).

For a better insight into sensitivity aspects of the noise matching condition in terms of component value tolerances, a new approach has been used. Firstly, applying the noise wave theory [22], $Z^*_{\rm opt}(\omega)$ is used as complex reference impedance and the source reflection coefficient Γ_S is derived. Secondly, the frequency response of Γ_S in terms of resonance frequency and bandwidth of the circuit in Fig. 3(c) is analyzed. Considering the circuit model in Fig. 3(c), $\Gamma_S(\omega)$ is [22]

$$\Gamma_S(\omega) = \frac{Z_S(\omega) - Z_{\rm opt}(\omega)}{Z_S(\omega) + Z^*_{\rm opt}(\omega)} \tag{3}$$

where the normalization impedance is the optimum noise impedance $Z_{\rm opt}$, i.e., a complex impedance. When the noise-matching condition (3) is achieved, $\Gamma_S(\omega) \approx 0$. However, for Z_S values diverging form the ideal value $Z_{\rm opt}$, (3) becomes

$$\Gamma_s(s) = \frac{s^2 + \frac{s(R_S - R_{\rm opt})}{L_S} + \frac{1}{(L_S C_{\rm opt})}}{s^2 + \frac{s(R_S + R_{\rm opt})}{L_S} + \frac{1}{(L_S C_{\rm opt})}} \tag{4}$$

where $s = j\omega$ denotes the complex frequency. Equation (4) is a classical second-order function, i.e., $\Gamma_S(\omega) = N(s)/D(s)$, which allows to express the denominator $D(\rm s)$ as $D(s) = s^2 + s(\omega)_0/Q + \omega_0^2$. Hence, from (4), the resonance frequency ω_0 and the quality factor of the equivalent network at the input of the active device under matching conditions [16], Q_{in} are

$$\omega_0^2 = \frac{1}{(L_S C_{\rm opt})} \tag{5}$$

$$Q_{in} = \frac{\omega_0 L_S}{(R_S + R_{\rm opt})} = \frac{1}{\omega_0 C_{\rm opt}(R_S + R_{\rm opt})}. \tag{6}$$

Near resonance, e.g., $\omega \approx \omega_0$, and for small matching errors ($R_S \approx R_{\rm opt}$), (4) becomes

$$\Gamma_S(s) \approx \frac{s^2 + \omega_0^2}{s^2 + \frac{s\omega_0}{Q_{in}} + \omega_0^2} = \frac{s^2 + \omega_0^2}{s^2 + sBW_{-3\ {\rm dB},in} + \omega_0^2}. \tag{7}$$

The input inherent -3 dB bandwidth under the near-to-noise matching condition [16] and fixed ω_0 can be expressed

$$BW_{-3\ {\rm dB},in} = \frac{\omega_0}{Q_{in}} = \frac{R_S + R_{\rm opt}}{L_S}. \tag{8}$$

Now, studying the sensitivity of ω_0 and $BW_{-3\ {\rm dB},in}$ sensitivity, rather than $\Gamma_S(\omega)$ sensitivity to component tolerances, permits a more practical approach to the sensitivity of any LNA amplifier to component tolerances.

Classically, the sensitivity of a network function $F(s)$ with respect to a parameter a is defined as

$$S_a^{F(s)}(s) = \frac{\frac{dF(s)}{F(s)}}{\frac{da}{a}} \tag{9}$$

where $dF(s)/F(s)$ is the relative variation of the function $F(s)$ due to parameter a variation da/a. Applying (9) to (5) and (8), the relative variation of ω_0 and $BW_{-3\ {\rm dB},in}$ in terms of component value variation is given by

$$\frac{\Delta\omega_0}{\omega_0} = S_{L_S}^{\omega_0}\frac{\Delta L_S}{L_S} + S_{C_{\rm opt}}^{\omega_0}\frac{\Delta C_{\rm opt}}{C_{\rm opt}} \tag{10}$$

$$\frac{\Delta BW_{-3\ {\rm dB},in}}{BW_{-3\ {\rm dB},in}} = S_{R_S}^{BW_{-3\ {\rm dB},in}}\frac{\Delta R_S}{R_S} + S_{L_S}^{BW_{-3\ {\rm dB},in}}\frac{\Delta L_S}{L_S} + S_{R_{\rm opt}}^{BW_{-3\ {\rm dB},in}}\frac{\Delta R_{\rm opt}}{R_{\rm opt}}. \tag{11}$$

Differentiating (5) and (8) with respect to real and imaginary components of Z_S, the resonance frequency and bandwidth sensitivity to R_S and X_S variation can be analytically derived

$$S_{L_S}^{\omega_0} = -0.5 \tag{12a}$$

$$S_{L_S}^{BW_{-3\ {\rm dB},in}} = -1 \tag{12b}$$

$$S_{R_S}^{BW_{-3\ {\rm dB},in}} = \frac{R_S}{R_S + R_{\rm opt}} \xrightarrow{@{\rm Matching}} \frac{1}{2}. \tag{12c}$$

Since the sensitivity of the resonance frequency and input inherent bandwidth due to Z_S variations are constants (-0.5, -1), $\Delta\omega_0/\omega_0$ and $\Delta BW_{-3\ {\rm dB},in}/BW_{-3\ {\rm dB},in}$ can be minimized *only* by the use of high-precision components, e.g., component values near to the designed values and small tolerances. Rewriting (10) and (11), while assuming zero variation of G_n, $R_{\rm opt}$ and $X_{\rm opt}$, one gets for the LNA circuit model in Fig. 3(c)

$$\frac{\Delta\omega_0}{\omega_0} = -0.5\frac{\Delta L_S}{L_S} \tag{13a}$$

$$\frac{\Delta BW_{-3\ {\rm dB},in}}{BW_{-3\ {\rm dB},in}} = \frac{R_S}{R_S + R_{\rm opt}}\frac{\Delta R_S}{R_S} - \frac{\Delta L_S}{L_S} \approx 0.5\frac{\Delta R_S}{R_S} - \frac{\Delta L_S}{L_S} \tag{13b}$$

Equations (13a) and (13b) show that any variation of the output impedance of the IMN (R_S and X_S) from the designed value $Z_S = Z_{\rm opt}$ due to component value tolerances will result in variations of the frequency response of $\Gamma_S(\omega)$, i.e., deviations of the frequency ω_0 and input inherent bandwidth $BW_{-3\ {\rm dB},in}$. Finally, this will result in deviation of the UWB LNA noise figure from the optimized design value.

C. Single-Section Versus Dual-Section Input Matching Network on Source Impedance Sensitivity

For given LNA bandwidth (BW) specification and properly chosen ω_0, the loaded Q-value Q can be calculated using $BW_{-3\ {\rm dB}} = \omega_0/Q$. Moreover, for a given transistor ($R_{\rm opt}$, $X_{\rm opt}$ at ω_0), the loaded Q-factor value of a single-section matching network, $Q = Q_I$ is given by [20], [21]

$$Q_I = \sqrt{\frac{R_G}{R_{\rm opt}} - 1}; \mathsf{R}_G > R_{\rm opt}. \tag{14}$$

For a dual L-section lossless matching network, the loaded Q-factor value of the matching network $Q = Q_{II}$ is [20], [21]

$$Q_{II} = \sqrt{\sqrt{\frac{R_G}{R_{\rm opt}}} - 1}; \mathsf{R}_G > R_{\rm opt}. \tag{15}$$

From (14) and (15) and for the same scaling ratio $R_G/R_{\rm opt}$, $Q_I > Q_{II}$.

The resistor ratio scaling conditions in (14) and (15) and the LNA bandwidth specification, usually confirm if a single- or a dual-section matching network should be used. However, if a dual-section matching network should be used, this has twice as many components compared to the single-section. After manufacturing, the resulting source impedance is a function of all these component values in the matching network and their tolerances, and it may deviate considerably from the designed value $R_S = R_{\rm opt}$. Therefore, the sensitivity of the source impedance, Z_S defined in Fig. 2, with regard to the Q-factor value for single- and dual-section matching networks will be analyzed.

For single- and dual-section matching networks, the source resistance R_S, can be expressed as a function of the generator resistance R_G and loaded Q-factor as $R_S = R_G(1 + Q_I^2)$ and $R_S = R_{\rm G}(1 + Q_{II}^2)^2$, respectively [20], [21]. Hence, the sensitivity functions for single- and dual-section matching networks become

$$S_{Q,I}^{R_S} = \frac{\frac{\Delta R_S}{R_S}}{\frac{\Delta Q_I}{Q_I}} = -\frac{2}{1 + \frac{1}{Q_I^2}} \tag{16}$$

$$S_{Q,II}^{R_S} = \frac{\frac{\Delta R_S}{R_S}}{\frac{\Delta Q_{II}}{Q_{II}}} = -\frac{4}{1 + \frac{1}{Q_{II}^2}}. \tag{17}$$

From (16) and (17) some practical aspects for the wideband amplifier design can be noted: 1) the sensitivity function accounting for matching condition increases with Q, and 2) low Q-values design of the amplifier matching networks improves not only the amplifier bandwidth but also its sensitivity to component value variations. The factor 4 in (17) indicates, however, that a dual-section matching network when compared with a single-section matching network could result in increased sensitivity of the resistive matching. In order to achieve simultaneously both low Q-values and low sensitivity the following condition can be deduced:

$$\left|S_{Q,II}^{R_S}\right| \le \left|S_{Q,I}^{R_S}\right| \rightarrow Q_{II}^2 \le \frac{Q_I^2}{2 + Q_I^2}. \tag{18}$$

Equations (13), (16)–(18) have the advantage of giving a first indication on how the frequency response of any matching network configuration loaded with a complex impedance will be affected by component value tolerances. For a given transistor and a specified bandwidth, they mainly result in first-hand RF amplifier design steps, in terms of deciding if single- or multi-section matching networks should be used. For example, the UWB LNA in this work has $R_{\rm opt}@4\ {\rm GHz} = 13\ \Omega$, and the bandwidth ${\rm BW}_{-10\ {\rm dB}} = 1.7\ {\rm GHz}$, where ${\rm BW}_{-10\ {\rm dB}} \approx BW_{-3\ {\rm dB}}/3$, (in RF design -10 dB rather than -3 dB is used for reflection coefficient value and bandwidth definition). Using (9) for the noise matching condition $|\Gamma_S| \approx -10\ {\rm dB}$, it results in the first $Q \le 0.8$. This value is less than the Q value of a single-section matching network transforming $R_G = 50\ \Omega$ to $R_{\rm opt} = 13\ \Omega$ as resulting from (1.1), i.e., $Q = 1.7$ and comparable with the Q value for a double-section matching network resulting from (2), i.e., $Q = 0.98$. Hence, a double-section input matching network must be used. Then, the R_S sensitivity relatively to Q-factor values, i.e., for single- and dual-section matching networks is easily calculated from (16) and (17).

III. Simulation Results

In order to get an accurate picture of how lumped component tolerances and manufacturing tolerances affect RF circuit performance, the lumped and distributed input matching networks of a dual-section UWB LNA [12], [13] are simulated and analyzed in this section. Fig. 4(a) shows the multisection input matching network configurations when the lumped passive components are used while Fig. 4(b) presents a distributed input matching network implemented with microstrip transmission lines. In order to follow the impedance transformation process from R_G to Z_S, four different reference planes are defined and equations corresponding to different impedance levels at these planes are derived. In these models, the lumped elements are characterized by their nominal value and typical tolerances for RF surface-mounted devices ($C_i \pm \Delta C_i$, $L_j \pm \Delta L_j$) [23], [24]. The distributed microstrip elements are characterized by the characteristic impedance Z_0 and their electrical length, θ_i, $i = 1, 2, 3, 4$, which are defined at the resonance frequency ω_0 as defined by (5). Printed circuit board process tolerances in terms of the microstrip transmission line width ($w \pm \Delta w$), length ($l \pm \Delta l$), substrate height ($h \pm \Delta h$), and dielectric permittivity ($\varepsilon_r \pm \Delta\varepsilon_r$) are considered. Ideally, the generator impedance, $R_G = 50\ \Omega$, is transformed to the optimum complex impedance $Z_{\rm opt}$ by the input matching network in Fig. 4(a) and (b) such that the minimum noise figure condition results in $Z_4 = Z_{\rm opt}$. Z_S variations due to lumped component tolerances are computed considering all possible combinations of the lumped element values. For the distributed elements, the width (Δw) and length (Δl) deviation due to

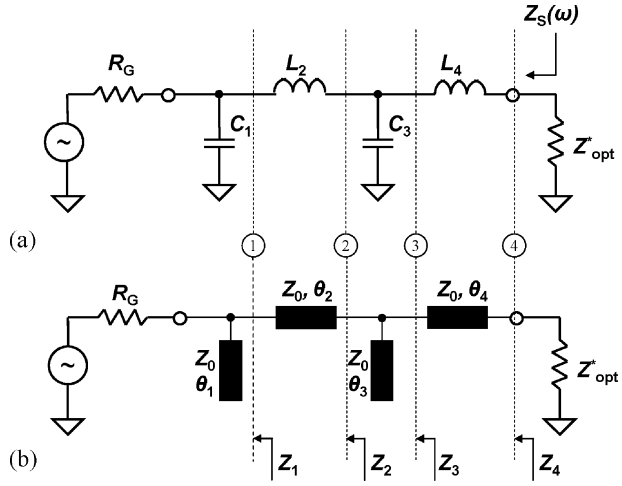

Fig. 4. Input matching network impedance transformation model: (a) lumped and (b) distributed.

photolithographic and etching processes are considered correlated, i.e., all transmission lines have the same width (narrow, nominal, large) and $\Delta l = \Delta w$. Then, the substrate height and dielectric permittivity deviations are considered for each case.

A. Lumped Input Matching Network Equations

The four impedances, Z_1 to Z_4 in Fig. 4(a) can be derived by means of iterative substitution in (19)–(22)

$$\begin{aligned} Z_1 &= R_1 + jX_1 \\ R_1 &= \frac{R_G}{(1+\omega^2 R_G^2 C_1^2)} \\ X_1 &= -\frac{\omega R_G^2 C_1}{(1+\omega^2 R_G^2 C_1^2)} \end{aligned} \tag{19}$$

$$\begin{aligned} Z_2 &= R_2 + jX_2 \\ R_2 &= R_1 \\ X_2 &= \omega L_2 + X_1 \end{aligned} \tag{20}$$

$$\begin{aligned} Z_3 &= R_3 + jX_3 \\ R_3 &= \frac{R_2}{[(1-\omega C_3 X_2)^2 + \omega^2 R_2^2 C_3^2]} \\ X_3 &= \frac{(X_2 - \omega R_2^2 C_3 - \omega X_2^2 C_3)}{[(1-\omega C_3 X_2)^2 + \omega^2 R_2^2 C_3^2)} \end{aligned} \tag{21}$$

$$\begin{aligned} Z_4 &= R_4 + jX_4 \\ R_4 &= R_3 \\ X_4 &= \omega L_4 + X_3. \end{aligned} \tag{22}$$

In this way, the dual-section impedance transformation is broken into several steps. The impedance deviation from the designed value can be followed from planes 1–4, showing in a simple way the cumulative effect of the passive component tolerances on the optimal noise matching condition.

B. Distributed Input Matching Network Equations

The open stub impedance $-jZ_0 \tan\theta_1$ [16] transforms R_G to the equivalent impedance Z_1 defined by

$$R_1 = Z_0 \frac{R_G Z_0}{Z_0^2 + R_G^2 \tan^2\theta_1} \tag{23}$$

$$X_1 = Z_0 \frac{-R_G^2 \tan\theta_2}{Z_0^2 + R_G^2 \tan^2\theta_1}. \tag{24}$$

The series transmission line then transforms Z_1 to Z_2 where R_2 and X_2 are defined as

$$R_2 = Z_0 \frac{R_1 Z_0 (1+\tan^2\theta_2)}{(Z_0 - X_1 \tan\theta_2)^2 + R_1^2 \tan^2\theta_2} \tag{25}$$

$$X_2 = Z_0 \frac{(X_1 + Z_0 \tan\theta_2)(Z_0 - X_1 \tan\theta_2) - R_1^2 \tan\theta_2}{(Z_0 - X_1 \tan\theta_2)^2 + R_1^2 \tan^2\theta_2}. \tag{26}$$

The generalized equations for open stub and series microstrip transmission line impedance transformation are

$$\begin{aligned} &R_{i+1}^{\text{openstub}} \\ &= Z_0 \frac{R_i Z_0}{(Z_0 - X_i \tan\theta_{i+1})^2 + R_i^2 \tan^2\theta_{i+1}} \end{aligned} \tag{27}$$

$$\begin{aligned} &X_{i+1}^{\text{openstub}} \\ &= Z_0 \frac{X_i (Z_0 - X_i \tan\theta_{i+1}) - R_i^2 \tan\theta_{i+1}}{(Z_0 - X_i \tan\theta_{i+1})^2 + R_i^2 \tan^2\theta_{i+1}} \end{aligned} \tag{28}$$

$$\begin{aligned} &R_{i+1}^{\text{TLseries}} \\ &= Z_0 \frac{R_i Z_0 (1+\tan^2\theta_{i+1})}{(Z_0 - X_i \tan\theta_{i+1})^2 + R_i^2 \tan^2\theta_{i+1}} \end{aligned} \tag{29}$$

$$\begin{aligned} &X_{i+1}^{\text{TLseries}} \\ &= Z_0 \frac{(X_i + Z_0 \tan\theta_{i+1})(Z_0 - X_i \tan\theta_{i+1}) - R_1^2 \tan\theta_{i+1}}{(Z_0 - X_i \tan\theta_{i+1})^2 + R_i^2 \tan^2\theta_{i+1}} \end{aligned} \tag{30}$$

Equations (27)–(30) show that the optimal noise matching condition at plane 4 depends on the variation of Z_0 and the electrical length of every transmission line in the network. The characteristic impedance Z_0 is related to the physical transmission line parameters and material properties, i.e., $Z_0 = f(\varepsilon_r, w, h)$ [16]. The electrical length is related to the physical length of the transmission line by $\theta_i = \beta_i$, where β is the propagation constant [16] and l_i is the length of every distributed element in Fig. 4(b).

C. Lumped Versus Distributed

For better comparison of the robustness of the lumped and distributed UWB LNA in Fig. 1(a) and (b), (19)–(30) are computed and the results are graphically represented in Fig. 5(a) and (b). The transformation processes from R_{G} to Z_{opt} using the nominal value of the lumped- or distributed-impedance are represented as traces on the Smith chart. The resulting impedance values at different planes in Fig. 4(a) and (b) and their variation due to passive component and manufacturing process tolerances are represented as normalized impedance values on the Smith chart. Detailed specification of the passive components is listed in Table I. Statistical simulations were performed with Advanced Design System (ADS2009) from Agilent Technologies Inc. Output noise figure variation due to lumped and distributed component tolerances over a large frequency range is shown in Fig. 6(a) and (b). As seen in Fig. 5(b) and Fig. 6(b), simulations taking typical printed circuit board process tolerances ($\pm 10\%$)

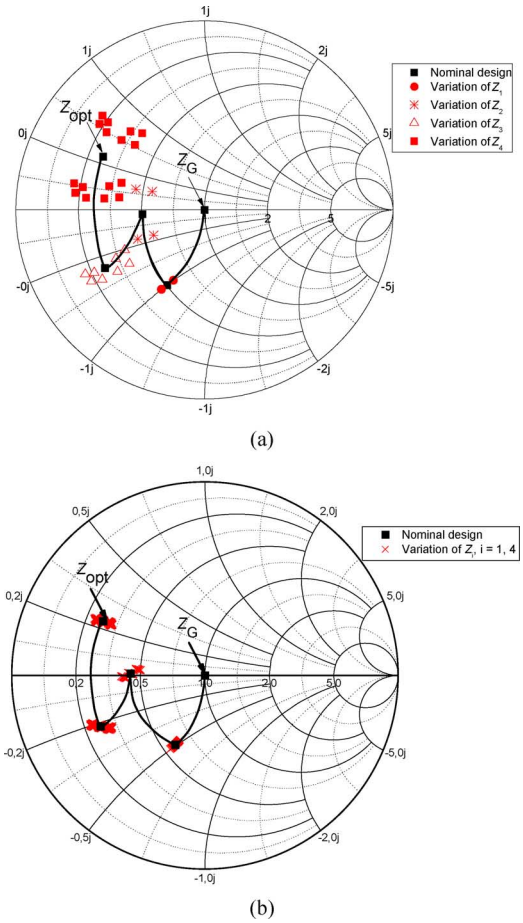

Fig. 5. Z_S sensitivity to input matching network component variations. (a) Lumped components ($C \pm 10\%$, $L \pm 10\%$). (b) Distributed components ($w = 0.542$ mm$\pm 10\%$, $l_i \pm 10\%$ w, $\varepsilon_r = 3.48 \pm 0.05$, $h = 0.254$ mm± 0.001 mm). Low-Q matching technique where $Q \approx 1$.

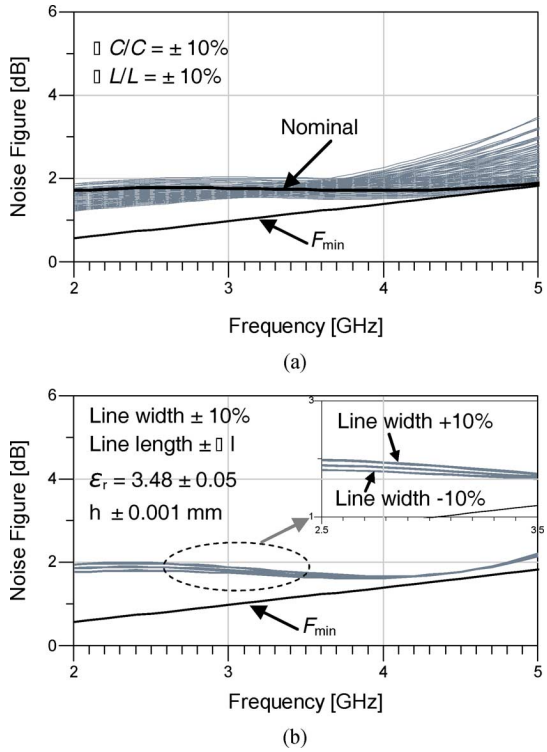

Fig. 6. Simulated noise figure of (a) lumped UWB LNA design, and (b) distributed UWB LNA design.

TABLE I
PASSIVE COMPONENT PARAMETERS

Lumped component name	Nominal value
C1	0.7 pF
L2	0.8 nH
C3	1.3 pF
L4	0.8 nH
Distributed component electrical length	**Nominal value @ 4.5 GHz**
θ_1	40.3°
θ_2	33.88°
θ_3	62.52°
θ_4	26.8°
Characteristic impedance	
Z_0	52.2 Ω

into consideration predict extremely low sensitivity of the noise figure of the UWB LNA, with a variation around the designed (nominal) value less than 0.6%. In contrast, as shown in Fig. 5(a) and Fig. 6(a), lumped element tolerances result in larger variation of the noise figure, e.g., 9.5% at 4 GHz.

Unlike the UWB LNA implemented with lumped elements, the LNA implemented with distributed matching networks using a conventional printed circuit board process shows an extremely low sensitivity to manufacturing process tolerances. Two main aspects related to the previous simulation results should be noted: 1) the need for experimental results to verify the low sensitivity of the distributed matching networks and 2) the need to understand why distributed matching networks provide robust performance of the LNA.

IV. EXPERIMENTAL RESULTS

Instead of manufacturing a large number of LNA modules—usually necessary when statistical analysis is performed—three different UWB LNA modules were fabricated to the purpose to compare with the simulation results. In these modules, the width of all microstrip lines (w) including the transmission lines in the bias network is purposely modified with $\pm 10\%$ around the designed nominal value. The $\pm 10\%$ variation corresponds to the width variations given in the manufacturer process data sheet. The three UWB LNA modules are thus: one corresponding to the *"nominal"* UWB LNA design that is characterized by the width of the transmission lines $w = 0.542$ mm for $Z_0 = 50\ \Omega$, and the other two UWB LNA modules where the width of the transmission lines is modified with $+10\%$ (*"large"*) and -10% (*"small"*). Then, the sensitivity of UWB LNA was evaluated in terms of transmission line width variation.

The photograph of the UWB LNA, including the broadband bias network using a butterfly radial stub [15] is presented in Fig. 7(a). The presented UWB LNA is designed for a noise figure below 4 dB and a flat transfer function over the 3.1–4.8 GHz bandwidth. The active device is MAX2649. For optimal wideband matching, the multisection wideband amplifier design is combined with the frequency-compensated

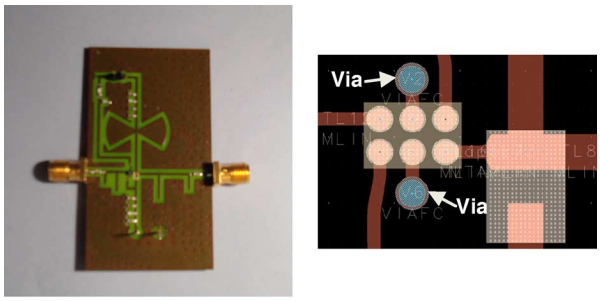

(a) (b)

Fig. 7. UWB LNA prototype: (a) Photograph of the UWB LNA (a) and (b) layout detail with LNA foot print and via contacts to the ground.

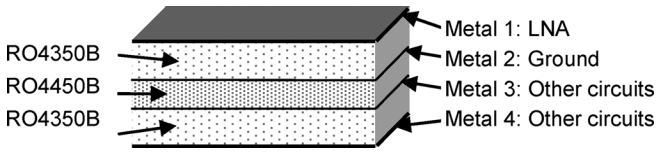

Fig. 8. Printed circuit board structure.

matching technique [16]. The matching networks are optimized at 4.5 GHz and the amplifier is unconditionally stable by means of a shunt stabilization resistor at the output [12]. Electromagnetic simulations were performed and the distributed input and output matching networks and the wideband bias network were optimized. Grounding-via analytical model in ADS was considered in schematic simulations. On layout level, via contacts to the ground seen in Fig. 7(b) were modeled as 2-D distributed layout components using electromagnetic simulator Momentum in ADS [25]. Simulated input reflection coefficient at 4.5 GHz is -10 dB. The UWB LNA is integrated into a four-layer board shown in Fig. 8. The topside of the board in Fig. 8 is dedicated to the UWB LNA, whereas the backside of the board to the rest of the UWB RF front-end [13]. The prototypes have a size of 23×50 mm.

The stack of the printed circuit board consists of two dual-layer RO4350B boards and a RO4450 prepreg, see Fig. 8.

Table II lists the printed circuit board parameters. Metal layers 1 and 4 are thicker than metal layers 2 and 3 because the surface layers are plated twice whereas the embedded metal layers 2 and 3 are plated once.

S-parameter measurements were done with a Rhode&Schwartz ZVM vector network analyzer. The Agilent N8974A Noise Figure Analyzer was used to measure the noise figure of the LNA. Fig. 9(a) and (b) shows the measured performances of the LNA.

Measured noise figure is less than 4 dB from 3.1 to near 4.8 GHz and follows the minimum noise figure of the device with some deviation at the upper frequency edge. This deviation corresponds to downward shift in frequency of the forward transfer function $|S_{21}|$ compared to the simulated $|S_{21}|$, as illustrated in Fig. 9(b). The measured forward transfer function $|S_{21}|$ is greater than 13 dB with a ± 0.5 dB variation. The supply voltage is 3 V and the consumed current is 13 mA. The input third-order intercept point (IIP3) is -6 dB at 4 GHz and 3.0 V supply.

TABLE II
PRINTED CIRCUIT BOARD PARAMETERS

Parameter (Rogers 4350B)	Dimension
Dielectric height	0.254 mm±0.001 mm
Dielectric constant	3.48±0.05
Dissipation factor	0.004
Parameter (Rogers 4450B)	**Dimension**
Dielectric height	0.200 mm
Dielectric constant	3.54±0.05
Dissipation factor	0.004
Parameter (Metal, common)	**Dimension**
Metal thickness, layer 1, 4	0.035 mm
Metal thickness, layer 2, 3	0.025 mm
Metal conductivity	5.8×10^7 S/m (Copper)
Surface roughness	0.001 mm

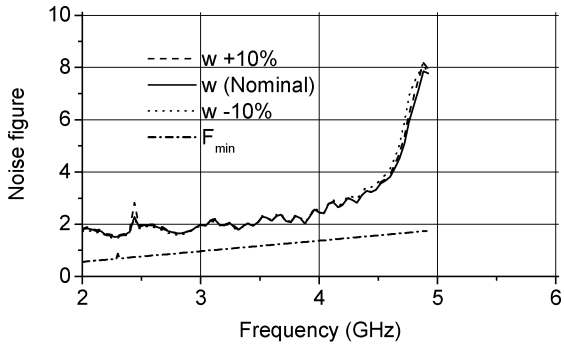

(a)

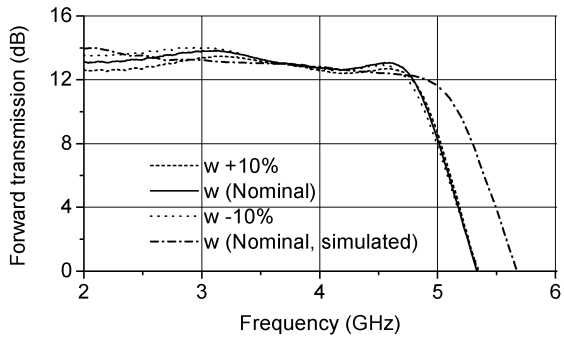

(b)

Fig. 9. Measured performance of the LNA: (a) measured noise figure, (b) measured forward transmission, when the microstrip line width varies $\pm 10\%$.

Using the simulated and measured results presented in Sections III and IV, the noise figure variance was calculated (variance $= \sigma^2$, where σ is the standard deviation from the mean value). For example, at 4 GHz and in the case of the low-noise amplifier implemented with distributed matching networks, the variance of the simulated noise figure was $\sigma^2_{\mathrm{sim,dist}} = 2.1 \times 10^{-3}$ and the variance of the measured noise figure was $\sigma^2_{\mathrm{meas,dist}} = 8.2 \times 10^{-3}$. In the case of the low-noise amplifier implemented with lumped matching networks, the simulated noise figure shown in Fig. 7(a) results in considerably higher values of the noise figure variance, i.e., $\sigma^2_{\mathrm{sim,lump}} = 82.7 \times 10^{-3}$.

V. CONCLUSION

The component tolerance effect on UWB LNA designs is studied and discussed in this work. A 3.1–4.8 GHz LNA ampli-

fier using distributed dual-section matching networks was presented. It was shown that the noise matching condition in its frequency response is sensitive to Z_S value variation from the designed value $Z_S = Z_{\rm opt}$ due to component value tolerances. It was demonstrated that lower LNA sensitivity can be achieved only by the use of high-precision passive components. For the dual-section UWB LNA the cumulative effect of passive component tolerances on the noise matching condition was modeled, calculated and compared for lumped and distributed matching networks. Simulations have shown large deviations from the target value of the noise figure when the dual-section UWB LNA was implemented with lumped matching networks. However, simulation and measurement results of the UWB LNA implemented with distributed microstrip matching networks showed a very robust performance, despite the $\pm 10\%$ variation of the line width.

One important conclusion of this study is that distributed impedance transformation process results in predictable and stable impedance values, near to the designed values. The low sensitivity of distributed passive components can be explained by low relative variation of the transmission line length $\Delta l/l$. For the UWB LNA presented in this work, assuming the same variation of the line length as for its width, the typical relative variation of the transmission line length was in the range of $\pm 0.35\%$–$\pm 0.9\%$.

In contradiction to the general conception that the organic printed circuit board technology has too large process variations for radio frequency circuit design, it was demonstrated in this study that a conventional printed circuit board can in fact enable the multisection matching networks UWB LNA with more passive components design, with low sensitivity to component tolerances.

ACKNOWLEDGMENT

Agilent Technologies Inc. is acknowledged for donation of Advanced Design System licenses and their long term support to Linköping University, Sweden.

REFERENCES

[1] B. Razavi, T. Aytur, C. Lam, F. R. Yang, K. Y. Li, R. H. Yan, H. C. Hang, C. C. Hsu, and C. C. Lee, "A UWB CMOS transceiver," *IEEE J. Solid-State Circuits*, vol. 40, no. 12, pp. 2555–2562, Dec. 2005.

[2] C.-W. Kim, M.-S. Kang, P. T. Anh, H.-T. Kim, and S.-G. Lee, "An ultra-wideband CMOS low-noise amplifier for 3–5-GHz UWB system," *IEEE J. Solid-State Circuits*, vol. 40, no. 2, pp. 544–547, Feb. 2005.

[3] J.-H. C. Zhan and S. S. Taylor, "A 5 GHz resistive-feedback CMOS LNA for low-cost multi-standard applications," in *IEEE Int. Solid-State Circuits Conf. Dig. Tech. Papers*, 2006, pp. 721–730.

[4] X. Guan and C. Nguyen, "Low-power consumption and high-gain CMOS distributed amplifiers using cascade of inductively coupled common-source gain cells for UWB systems," *IEEE Trans. Microwave Theory Tech.*, vol. 54, no. 8, pp. 3278–3283, Aug. 2006.

[5] C. Grewing, M. Friedrich, G. L. Puma, C. Sander, S. van Waasen, A. Wiesbauer, and K. Winterberg, "Fully integrated ultra wide band CMOS low-noise amplifier," in *Proc. 30th Eur. Solid-State Circuits Conf.*, 2004, pp. 435–438.

[6] A. Bevilacqua and A. M. Niknejad, "An ultrawideband CMOS low-noise amplifier for 3.1–10.6 GHz wireless receiver," *IEEE J. Solid-State Circuits*, vol. 39, no. 12, pp. 2259–2268, Dec. 2004.

[7] A. Ismail and A. Abidi, "A 3–10 GHz low-noise amplifier with wideband LC-ladder matching network," *IEEE J. Solid-State Circuits*, vol. 39, pp. 2269–2277, Dec. 2004.

[8] M. Karlsson and S. Gong, "A frequency-triplexed inverted-F antenna system for ultra-wide multi-band systems 3.1–4.8 GHz," *ISAST Trans. Electron. Signal Process.*, vol. 1, no. 1, pp. 95–100, 2007.

[9] M. Karlsson and S. Gong, "Circular dipole antenna for Mode 1 UWB radio with integrated balun utilizing a flex-rigid structure," *IEEE Trans. Antennas Propag.*, vol. 57, no. 10, pp. 2967–2971, Oct. 2009.

[10] M. Karlsson, P. Hakansson, and S. Gong, "A frequency triplexer for ultra-wideband systems utilizing combined broadside- and edge-coupled filters," *IEEE Trans. Adv. Packag.*, vol. 31, no. 4, pp. 794–802, Nov. 2008.

[11] A. Serban and S. Gong, "Low-noise amplifier design at 5 GHz," in *Proc. IMAPS Nordic Annu. Conf.*, Tønsberg, Norway, 2005, pp. 227–229.

[12] A. Serban and S. Gong, "Ultra-wideband low-noise amplifier design for 3.1–4.8 GHz," in *Proc. GigaHertz 2005 Conf.*, Uppsala, Sweden, pp. 291–294.

[13] A. Serban, M. Karlsson, and S. Gong, "A frequency-triplexed RF front-end for ultra-wideband systems," *ISAST Trans. Electron. Signal Process.*, vol. 2, no. 1, pp. 83–88, 2008.

[14] A. Serban, M. Karlsson, and S. Gong, "All-microstrip design of three multiplexed antennas and LNA for UWB systems," in *Proc. IEEE Asia-Pacific Microwave Conf.*, Dec. 2006, pp. 1109–1112.

[15] A. Serban, M. Karlsson, and S. Gong, "Microstrip bias networks for ultra-wideband systems," *ISAST Trans. Electron. Signal Process.*, vol. 2, no. 1, pp. 16–20, 2008.

[16] R. Ludwig and P. Bretchko, *RF Circuit Design. Theory and Applications*. New York: Prentice Hall, 2000, pp. 502–504.

[17] G. Gonzalez, *Microwave Transistor Amplifier Analysis and Design*. Upper Saddle River, NJ: Prentice-Hall, 1997, pp. 344–352.

[18] A. Nieuwoudt and Y. Massoud, "Variability-aware multi-level integrated spiral inductor synthesis," *IEEE Trans. Comput.-Aided Design Integr. Circuits Syst.*, vol. 25, no. 12, pp. 2613–2625, Dec. 2006.

[19] J. Dobes and Z. Kolka, "Enhanced modes of the sensitivity analysis for RF design," in *Proc. IEEE 30th Eur. Solid-State Circuits Conf.*, 2004, pp. 435–438.

[20] T. H. Lee, *RF Circuit Design. The Design of CMOS Radio-Frequency Integrated Circuits*, 2nd ed. Cambridge, U.K.: Cambridge Univ. Press, 2004, pp. 92–93.

[21] C. Bowick, *RF Circuit Design*. London, U.K.: Newnes, 1997, pp. 72–75.

[22] P. Penfield Jr., "Wave representation of amplifier noise," *IRE Trans. Circuit Theory*, vol. 9, no. 1, pp. 84–86, Mar. 1962.

[23] Chip Inductors Product Catalog Toko, Selection Guide: Chip inductor type: LL1005FHL [Online]. Available: http://www.toko.com

[24] Chip Monolithic Ceramic Capacitors Product Catalog Murata, Capacitors type: GJM Series [Online]. Available: http://www.murata.com

[25] Advanced Design Systems (ADS) Agilent Technologies Inc. [Online]. Available: http://eesof.tm.agilent.com/

Adriana Serban received the M.Sc. degree in electronic engineering from Politehnica University, Bucharest, Romania. She is working toward the Ph.D. degree in communication electronics.

From 1981 to 1990, she was with Microelectronica Institute, Bucharest, Romania, being involved in mixed integrated circuit design. From 1992 to 2002, she was with Siemens AG, Munich, Germany, and with Sicon AB, Linkoping, Sweden as analog and mixed signal integrated circuit Senior Design Engineer. Since 2002 she has been a Lecturer at Linkoping University teaching in analog/digital system design, RF system design, and microwave engineering. Her main research and work interest has been RF circuit design, high-speed data transmissions, and high-speed integrated circuit design.

Magnus Karlsson was born in Västervik, Sweden, in 1977. He received the M.Sc., Licentiate of Engineering, and the Ph.D. degrees from Linköping University, Norrkoping, Sweden, in 2002, 2005, and 2008, respectively.

In 2003 he started in the Communication Electronics Research Group at Linköping University and is currently working as a Senior Researcher. His main work involves wideband antenna-techniques, wideband transceiver front-ends, and wireless communications.

Shaofang Gong (M'03) was born in Shanghai, China, in 1960. He received the B.Sc. degree from Fudan University, Shanghai, China, in 1982, and the Licentiate of Engineering and Ph.D. degrees from Linköping University, Norrkoping, Sweden, in 1988 and 1990, respectively.

Between 1991 and 1999, he was a Senior Researcher at the Microelectronic Institute–Acreo in Sweden. From 2000 to 2001 he was the Chief Technology Officer at a spin-off company from the institute. Since 2002 he has been Professor in Communication Electronics at Linköping University. His main research interest has been communication electronics, including RF design, wireless communications, and high-speed data transmissions.